Time-Resolved X-Ray Radiography of Diesel Injectors from the Engine Combustion Network

A.L. Kastengren[1], F.Z. Tilocco, D. Duke, C. F. Powell
Energy Systems Division, Argonne National Laboratory; Argonne, IL USA
akastengren@anl.gov

Seoksu Moon[2], Xusheng Zhang
X-Ray Science Division, Advanced Photon Source, Argonne National Laboratory

Abstract

A significant hurdle to the understanding of sprays is the link between nozzle geometry and the fluid distribution in the spray. X-ray radiography can help to clarify this link by providing quantitative measurements of the spray density in the near-nozzle region, including at the exit plane. The current work describes x-ray radiography measurements performed at Argonne National Laboratory under the "Spray A" conditions of the Engine Combustion Network. Four injector samples have been studied, and model-dependent reconstructions have been used to generate 3-D maps of the average fuel density as a function of time. These measurements reveal differences between the sprays from nominally identical injectors which can be interpreted in terms of geometric differences in the injector nozzles that have been measured previously.

Introduction

Due to the importance of fuel and air mixing in practical diesel combustion, diesel sprays have been the object of research interest for many years. Several optical techniques have been used to characterize spray parameters under both combusting and non-combusting conditions, including spray penetration [1], cone angle, liquid length[2], flame liftoff length[3], and the velocity field surrounding the spray[4]. While these diagnostics have provided important insights regarding spray behavior, they have provided only limited data regarding the internal structure of sprays. The numerous small spray droplets in diesel sprays create a flowfield with high optical density. Advanced optical diagnostics have been attempted on diesel sprays to overcome the optical density limitations, though with only limited success [5,6].

A significant problem in previous diesel spray research has been the difficulty of comparing results from different experiments. For example, nozzle geometry is known to strongly affect spray structure. However, due to the small size (~ 100 μm) of diesel spray nozzles, it is difficult to characterize the nozzle geometry in detail [7]. The Engine Combustion Network (ECN) was conceived to remove this impediment to diesel spray research. A series of nominally-identical injectors have been characterized under well-defined conditions by a variety of institutions. These efforts have already yielded fruit in showing both the importance of matching all pertinent experimental parameters and the ability to achieve good agreement between different institutions on parameters of interest in diesel sprays [8].

The current study uses x-ray radiography to probe a non-vaporizing version of the Spray A ECN condition. Radiography has been used for several years to characterize the near-nozzle distribution of fuel sprays under a wide variety of conditions [9-11]. The current radiography data will be used to describe the development of the spray velocity, shape, and density with downstream distance. Important differences between the nominally-identical ECN injectors will also be described.

Experimental Methods

The x-ray radiography experiments in this work were performed at the 7BM beamline of the Advanced Photon Source (APS) at Argonne National Laboratory. The beamline layout and performance are described elsewhere [12]. A monochromatic beam of x-rays at 8 keV photon energy was focused to a 5 x 6 μm FWHM focus size to probe the spray with high spatial resolution. The incident x-ray flux on the detector was approximately 2.6 x 10^{10} ph/s.

The radiography measurements represent a pathlength-integrated measure of the fuel density along one beam path through the spray. To measure the spatial distribution of the fuel, a two-dimensional raster-scan approach is used, with each point measured from a different set of spray events. To further improve the signal/noise in the final data, each data point is an average of 128-256 individual spray events. Measurements of

[1] Corresponding Author
[2] Current Affiliation Combustion and Engine Research Team, AIST, Ibaraki, Japan

the needle lift of these injectors [13] and of spray events from a similar injector [9] have shown that shot-to-shot variations are likely to be fairly minor. As such, the spray data shown in this work represent the persistent, ensemble-averaged behavior of the spray, rather than the precise structure of any one spray event. The coordinate system used in this work is illustrated in Fig. 1.

When the data were processed, the signal was binned for each cycle of the APS (i.e., 3.68 μs). Due to the use of monochromatic x-rays, the conversion of x-ray transmission to fuel mass is relatively simple. A simple Beer's Law approach can be used; the projected density of the spray M (in mass/area) can be calculated from the fuel absorption coefficient (μ), the x-ray intensity during the spray (I) and before the spray (I_0) using Eq. 1.

$$I = I_0 e^{-\mu M} \quad (1)$$

In order to provide useful data for comparison with other ECN experiments, the experimental conditions have been matched as closely as possible to the ECN Spray A specification [14]. The specified injectors, fuel, rail, and injection line lengths were used. There are three main deviations of the current experimental conditions from the Spray A specification. While the Spray A specification references the actual injection duration, in the current measurements the commanded injection duration was fixed. Furthermore, a somewhat different current waveform was used for the 210675 injector (200 μs at 18 A, 550 μs at 12 A) than the other injectors (450 μs at 18 A, 345 μs at 12 A). Second, the ambient gas for these experiments was nitrogen gas at room temperature, rather than the high-temperature post-combustion gas mixture specified. This is largely due to the x-ray transparent polymer windows used in these experiments, which cannot be used at high temperatures. The current experiments have, however, matched the ambient density of the Spray A specification, at the expense of not matching the ambient pressure; density is expected to be a more critical parameter in fuel-air mixing than pressure [1]. Finally, the injector tip temperature for these experiments was approximately 60° C, rather than the 90° C specification. For these measurements, the injector was housed in a heated flange maintained at 65-70° C to match the injector body temperature used in previous Spray A experiments. Thermocouple measurements on the tip showed that thermal conduction through the injector caused the tip temperature to remain nearly the same as the injector body.

Results and Discussion

In the interest of brevity, only the quasi-steady state spray behavior will be described in this work. For each viewing angle of the spray, the radiography data provide a two-dimensional projection onto a plane of the actual three-dimensional fuel mass distribution as a function of time. Figure 2 shows a typical quasi-steady state spray distribution. The spray is narrow and of high density near the nozzle, fanning out to a broader, low density plume at more downstream positions.

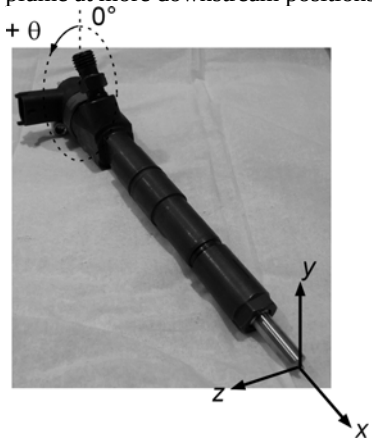

Figure 1. Illustration of measurement coordinate system.

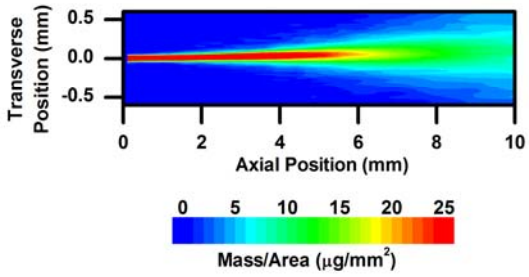

Figure 2. Projected mass distribution for nozzle 210679 681 μs after start of injection (SOI), during the steady-state portion of the spray development.

While the structure seen in Fig. 2 is typical of that seen for all of the Spray A cases, there are significant differences between the nozzles and between different viewing angles for the same injector. Figure 3a shows the distribution of projected density across the spray for one of the nozzles (210677) at the four different viewing angles. The spray appears to have a significantly different structure depending on the view examined. Viewing angles -30°and 0° appear narrow and strongly peaked, while the +60° and +90° views appear much broader. It should be noted that these projections all represent different views of the same object, namely the three-dimensional fuel mass distribution. The marked differences between these distributions indicate a high degree of asymmetry in the spray plume. Figure 3b shows the projected density at one downstream position (x = 4 mm) for the four Spray A cases at a single viewing angle. There are several significant differences between the

nozzles. A three-dimensional reconstruction is needed to separate the influence of spray asymmetry from true differences between the sprays. However, the spray from nozzle 210678 appears bimodal in this view, which is quite different than the other nozzles, and indicates a highly non-ideal spray pattern.

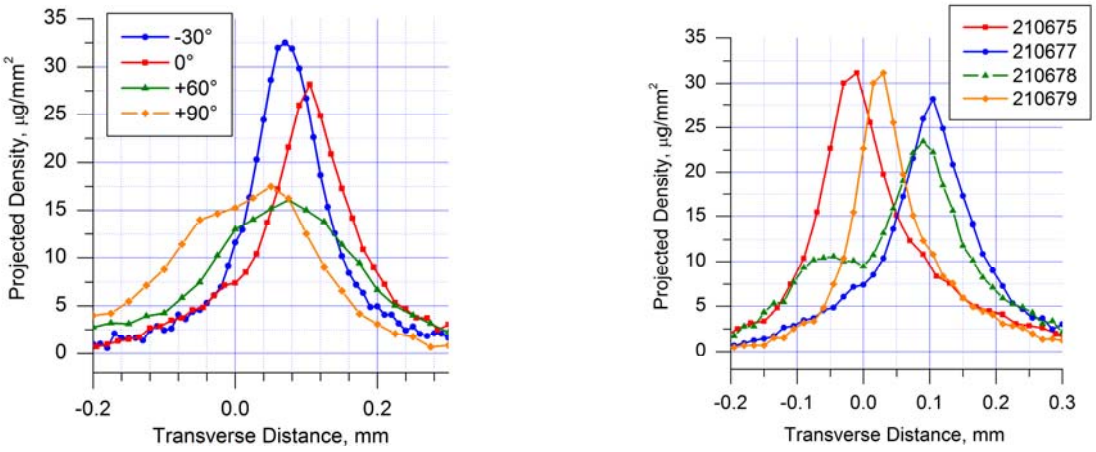

a) **b)**

Figure 3. Comparison of projected density across the spray axis at x = 4 mm for a) the four viewing angles for nozzle 210677, b) the four Spray A nozzles at the 0° viewing angle.

Spray Velocity

The mass distribution data can be used to describe trends in the spray velocity under quasi-steady state conditions. As has been described elsewhere, the integral of the projected density across the spray axis (the transverse integrated mass, or TIM) is inversely proportional to the mass-averaged spray velocity at a given x [10]. This can be used to understand how the spray velocity decays with downstream distance. Figure 4 shows the trend in velocity with x. As this analysis only shows relative velocities between different axial positions, the data have been normalized by the minimum TIM (maximum velocity) location. The velocity trends for all of the nozzles are quite similar, and show a steady decline in spray velocity with downstream distance. The velocity is substantially less than half of the initial velocity in the region of the liquid length (approximately x = 11 mm) [8].

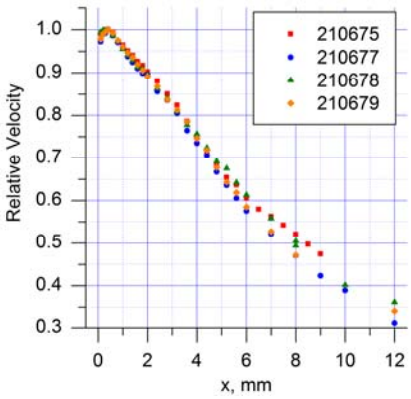

Figure 4. Trend in mass-averaged spray velocity with downstream distance.

Near-Nozzle Fuel Distribution

The mass distribution data can be used directly to understand the amount of mass present immediately outside the nozzle exit. The integral of the projected density across the spray axis (the transverse integrated mass, or TIM) can be converted to an equivalent diameter of void-free liquid given the liquid density. Table 1 shows the average TIM across the four orientations for each nozzle at x = 0.1 mm, the nearest measurement position to the nozzle, as well as the equivalent diameter calculated assuming a liquid density of 715 kg/m^3 and the nozzle diameter measured with optical microscopy [14]. The trends in measured nozzle diameter are largely preserved in the current equivalent diameter data. However, all of the equivalent diameter values are somewhat less than the measured nozzle diameter. These data would indicate that either the diameter of the liquid jet is less than

the measured nozzle diameter, that the fuel density is slightly less than the assumed value of 715 kg/m^3 (potentially due to voids), or some combination of these two effects.

While the 2D raster scan approach provides a wealth of data regarding the spatial distribution of spray mass, it represents a projection onto a plane of the true three-dimensional spray structure. To further understand the spray structure, radiography data were obtained from four different viewing angles (-30°, 0°, +60°, and +90° rotations about the injector axis). While this does not represent a complete dataset for tomography [15], it provides sufficient data for a model-based reconstruction [11]. In order to further smooth the data for accurate fitting, the radiography data have been binned over 25 time steps (92 µs), which greatly reduces noise in the measurements. For this work, the reconstruction is performed at a time 680 µs after SOI, which is in the quasi-steady region near the middle of the injection event.

Table 1. TIM, equivalent diameter, and measured exit diameter for the Spray A nozzles.

Nozzle	TIM	Equivalent D	Measured Exit D
	µg/mm	µm	µm
210675	4.17 ± 2%	86 ± 1%	89.4 ± 1
210677	3.61	80	83.7
210678	4.03	85	88.6
210679	3.77	82	84.1

These reconstructions provide a wealth of information regarding the spray structure. Near the nozzle, the assumed distribution is an elliptical core region of constant density; the fitting procedure is used to determine the size, shape, orientation, and density of this core region. The results of this analysis are shown in Table 2. The reconstructed size of the spray is quite similar to the equivalent diameter from above and the microscopic imaging of the nozzle exit, though the reconstruction consistently predicts a larger eccentricity than the microscopy of the nozzle exit. Interestingly, the reconstruction and microscopy give similar values for the orientation of the major axes of the distributions, which lends confidence that the reconstruction is accurately describing the spray distribution. The density value from the reconstruction is somewhat lower (by less than 10 %) than the bulk liquid density. Part of this difference is caused by small deviations between the measured distributions and the fitted curves due to a slight tail to the experimental distribution that is not captured properly with the fitting procedure, as shown in Fig. 5a.

Table 2. Comparison of spray reconstruction and optical microscopy of nozzle exit.

	210675	210677	210678	210679
Major Axis, µm	90.4 ± 0.5	88.6	90.7	87.7
Minor Axis, µm	81.3	76.8	79.1	78.5
Major Axis Orientation, °	91 ± 2	65	17	95
Density, kg/m^3	678	659	693	665
Microscopy Major Axis, µm	92.9	86.8	89.3	85.5
Microscopy Minor Axis, µm	85.9	80.5	87.6	82.4
Microscopy Orientation, °	66	65	42	83

The mass distribution of the spray becomes more complex at more downstream positions. Figure 5b shows the projected density vs. y for nozzle 210677 at x = 6 mm. A simple Gaussian curve is a rather poor fit to the experimental data, which feature a sharper peak and wider tails than a Gaussian. As such, fits have been performed using the sum of two Gaussian curves (one narrow to capture the peak, and one wider to capture the tails), which provides an excellent fit to the experimental data.

Figure 6 shows the reconstructions of the spray distribution for nozzle 210677 at x = 6 and 10 mm. Several trends are evident. First, the distribution is highly elliptical. The orientation of the major axis matches that of the reconstruction at x = 0.1 mm and the microscopy of the nozzle exit, indicating that nozzle exit eccentricity likely leads directly to spray eccentricity. The density distribution does not demonstrate a simple Gaussian behavior, as would be the case with a single-phase turbulent jet [16]. The distributions are instead much more strongly peaked. The narrow Gaussian used in fitting seems to represent a core of relatively high density (containing 40% of the spray mass in this cross-section) surrounded by a lower-density sheath, which corre-

sponds to the broader Gaussian used in the fitting. This structure does not necessarily indicate a sharp boundary between the two regions, but is used as a guide for understanding the differences between high- and low-density regions of the spray.

At more downstream positions, the plume becomes larger, causing the density to decrease, and the core region to become less distinct. At the most downstream positions measured, a simple Gaussian curve provides a good fit to the experimental projections; as such, the core-sheath structure is absent. The distribution also remains eccentric, and in the same orientation seen at more upstream positions. The other nozzles measured show similar behavior, though the orientation of the major axis of the distribution varies from nozzle to nozzle.

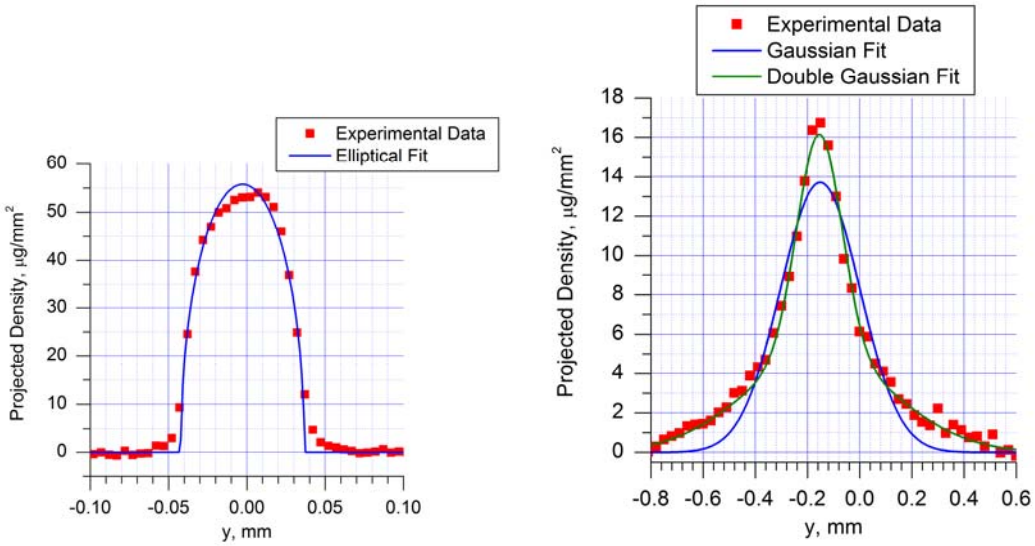

a) **b)**

Figure 5. Experimental density vs. *y* and fits for nozzle 210677, 0° viewing angle at a) *x* = 0.1 mm, b) *x* = 6.0 mm.

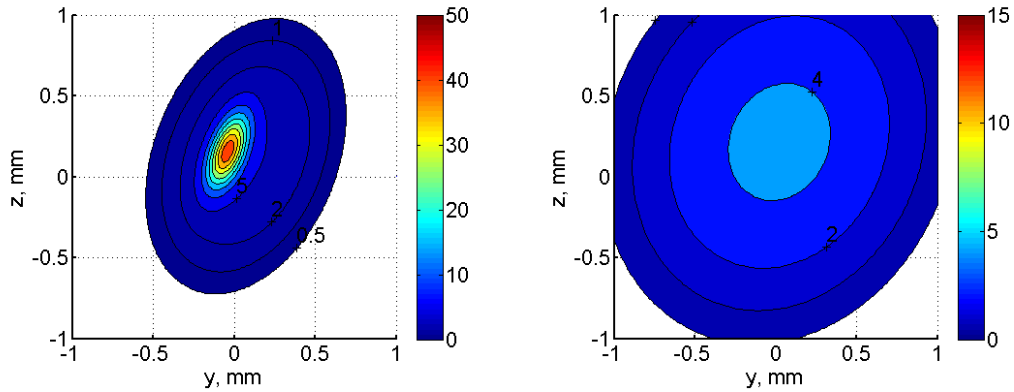

a) **b)**

Figure 6. Reconstruction of steady-state liquid density (in kg/m^3) for nozzle 210677 at a) *x* = 6 mm and b) *x* = 10 mm.

This structure has profound implications. The eccentricity of the spray will have little impact on measurements that are integrated across the entire cross-section of the spray (i.e., spray penetration, liquid length, or flame liftoff length). However, for other diagnostics (for example, planar measurements of spray properties), the orientation of the spray will have a significant impact on the measurements. Furthermore, while traditional measures of spray width (cone angle based on thresholding of spray shadowgraphs or schlieren) focus on the periphery of the spray, in the near-nozzle region, there is significant internal structure in the spray that is not adequately captured by these measures.

As the spray moves downstream, the fraction of the spray mass in the core region changes significantly. To quantify the amount of fuel in the core vs. sheath regions, the area of the Gaussian curve used to fit the core region of the projection is compared to the total integral of the projection at a given *x*. Figure 7 shows the fraction of the spray mass found in the core region as a function of downstream distance. For all nozzles, less than half of the mass in a given cross-section resides in the core region, though the core represents a significant fraction of the total mass. The fraction of mass in the core region declines monotonically for all nozzles except for nozzle 210679. By x = 12 mm, the core region is indistinguishable from the sheath for all of the sprays. This may be due to either shot-to-shot variations in the spray density (causing a smearing of the core region when the data are averaged) or the downstream distance simply becoming great enough that the core mixes well with the surrounding fluid.

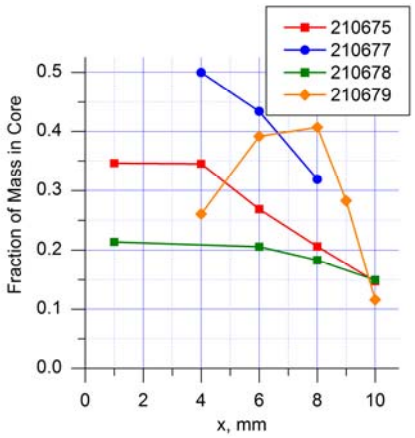

Figure 7. Fraction of the liquid mass in the core region for given *x* positions in the sprays from the ECN Spray A nozzles.

While the central region of the spray occupies only a small region of space, due to its relatively high density, it contains a significant fraction of the spray mass. The reconstructions of spray density can be used to better understand how much fuel resides at various density levels. Such a plot is useful in understanding the fraction of the fuel that resides in rich vs. lean regions. For the specified Spray A conditions, a fuel density of 1 kg/m^3 represents approximately stoichiometric conditions. Thus, regions of density greater than 1 kg/m^3 represent fuel-rich regions, while areas of density less than 1 kg/m^3 represent lean regions. It should be noted that, as the current experiments were performed at room temperature, the spray structure may be different than that found under vaporizing and combusting conditions.

Figure 8 shows histograms of the fraction of fuel residing in regions of different density for nozzle 210679 at x = 6 and 12 mm. At x = 6 mm, the vast majority of the fuel mass is in rich regions. This position is upstream of the experimental liquid length, so the fuel in the densest regions of the spray at this position would not be completely vaporized. The peak density at this position is approximately 7% of the bulk liquid density. As discussed in previous work [11], to properly calculate the drag coefficient on droplets at this density level, the influence of nearby droplets must be accounted for. A small fraction of the fuel resides in lean and stoichiometric regions. These regions are at the periphery of the spray, presumably in regions of low velocity and mass flux.

At x = 12 mm, the density values have fallen precipitously compared to x = 6 mm. This position is downstream of the liquid length seen in vaporizing spray measurements [8], so under vaporizing conditions, all of the fuel would be in the gas phase at this position. Approximately ¼ of the fuel resides in lean regions. The majority of the fuel (> 60%) still lies in fuel-rich regions. However, the peak density at this x position is only a few times that for a stoichiometric mixture.

In order to compare the current data to more traditional measures of spray development, such as liftoff length and liquid length, the trend in the liquid density with downstream distance is required. Figure 8 shows the trend in the peak density of the reconstructions vs. x for the four Spray A nozzles. It should be noted that the peak density value is quite sensitive to the fit parameters for the core region, which is quite narrow, and hence dependent on only a small fraction of the measured points at any x position. Thus, these density values should be considered an approximation. Comparisons between the nozzles show that the larger nozzles (210675 and 210678) have a higher peak density than the smaller diameter nozzles (210677 and 210679) throughout the x range examined. While the density values for the different nozzles show some differences, all of the nozzles show the same trend. The peak density in the spray plume declines rapidly with downstream

distance. As the trend appears linear on the semilog scale used in Fig. 8, exponential fits were performed on the datasets. For all of the nozzles, the decay constant was approximately 0.5 mm^{-1}.

The rapid decrease of liquid density with downstream distance has several implications. The first regards the liquid length. It has been assumed in the literature that the liquid length is mixing limited [17]; thus, the liquid length would be expected to occur when the peak density as a function of x reaches a threshold value, which depends on the ambient environment and liquid properties. Due to the rapid decrease in fuel density with downstream distance, relatively large differences in fuel density between nozzles at a given x will result in only minor differences in the liquid length. As such, the liquid length will be relatively insensitive to variations in spray density between nozzles. It should be noted that comparisons between the current data (taken under non-vaporizing conditions) and vaporizing spray data must be performed with care.

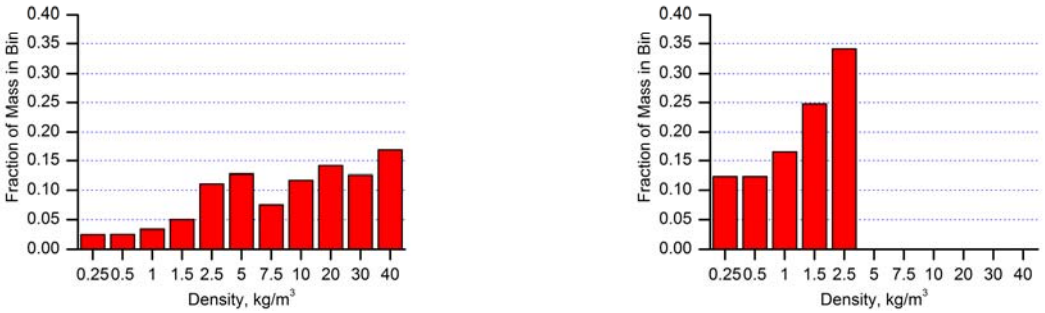

Figure 7: Histogram of fraction of fuel mass residing at different density levels for nozzle 210679 at a) x = 6 mm and b) x = 12mm.

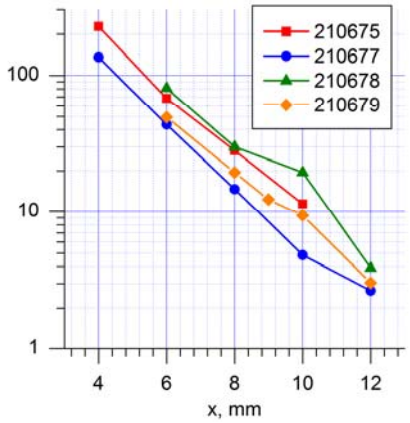

Figure 8: Trends in peak density in a spray cross-section vs. x for the ECN Spray A nozzles.

The trend in spray width with downstream distance is an important parameter in understanding the spray dispersion. Figure 9 shows measures of the major and minor axis sizes of the reconstructions (core and sheath) for nozzle 210677 as x is varied; the results for the other Spray A nozzles are similar. For x < 4 mm, the experimental profiles are complex and difficult to fit; for x > 8 mm, the core region becomes indistinguishable from the sheath region, so a simpler distribution assuming only a sheath region is used in the reconstruction. All measures of the spray width increase with downstream distance. The rate of increase is roughly linear, as is expected for a turbulent jet [16]. For the sheath region, the major and minor axes grow at similar rates. This results in a lower eccentricity of the spray with downstream distance, though some eccentricity remains even at the most downstream distance reconstructed (x = 12 mm).

Summary and Conclusions

X-ray radiography has been used to examine the quasi-steady state behavior of the ECN Spray A condition. The experiments have been performed under room-temperature conditions, but have otherwise largely matched the Spray A specification, including the ambient density. Analysis of the trends in the spray velocity show that the spray velocity decreases to half of the nozzle exit velocity by x = 8 mm, with all nozzles showing similar trends. Three-dimensional reconstructions of the spray distributions show the spray structure at various down-

stream positions, with a nearly intact liquid core indicated near the nozzle exit, a sharply peaked density distribution for x = 4-10 mm, and a smoother density distribution for x > 10 mm. The density distributions are highly eccentric for all of the Spray A cases, with the eccentricity apparently tied to imperfections in the nozzle geometry. Both the average and peak density in the plume rapidly diminish as x increases, which has important implications regarding the measurement of spray liquid length. The spray width grows approximately linearly for x > 4 mm, in agreement with previous measurements of turbulent jets.

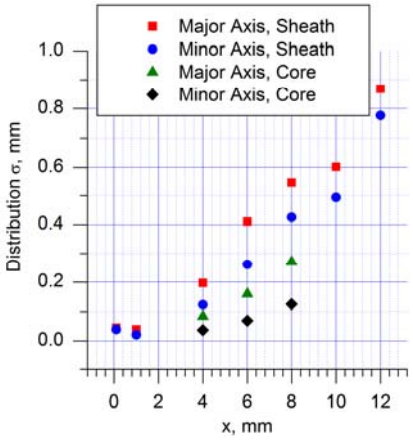

Figure 9: Trends in various measures of spray width vs. x for the 210677 injector.

Acknowledgements

This work was performed at the 7BM beamline of the Advanced Photon Source, Argonne National Laboratory. The use of the APS is supported by the U.S. Department of Energy under Contract No. DE-AC02-06CH11357 and by the DOE Vehicle Technologies Program, with Gurpreet Singh as Team Leader.

References

[1] Naber, J. and Siebers, D., *SAE Paper 960034* (1996).
[2] Siebers, D., *SAE Paper 980809* (1998).
[3] Pickett, L. and Siebers, D., *Combustion and Flame*, 138:114-135 (2004).
[4] Cossali, G. E., Gerla, A., Coghe, A., and Brunello, G., *SAE Paper 960862* (1996).
[5] Leick, P., Grzeszik, R., Arndt, S., and Wissel, S., *24th Annual ILASS-Europe Conference*, Estoril, Portugal (2011).
[6] Linne, M., Paciaroni, M., Hall, T., and Parker, T, *Experiments in Fluids*, 40:836-846 (2006).
[7] First International Workshop of the Engine Combsution Network, ECN1, Ventura CA (2011).
[8] Pickett, L. M., Genzale, C., Bruneaux, G., Malbec, L.-M., Hermant, L., Christiansen, C., and Schramm, J., *SAE Paper 2010-01-2106* (2010).
[9] Kastengren, A., Powell, C. F., Wang, Y.-J., and Wang, J., *Journal of Engineering for Gas Turbines and Power*, 130:032811 (2008).
[10] Kastengren, A., Powell, C. F., Wang, Y.-J., Im, K.-S., and Wang, J., *21st Annual ILASS Conference*, Orlando, FL (2008).
[11] Kastengren, A., Powell, C. F., Liu, Z., and Wang, J., *SAE Paper 2009-01-0840* (2009).
[12] Kastengren, A., Powell, C.F., Arms, D., Durfresne, E. M., and Wang, J., *22nd Annual ILASS Conference*, Cincinnati, OH (2010).
[13] Kastengren, A., Tilocco, F. Z., Powell, C. F., and Fezzaa, K., *23rd Annual ILASS Conference*, Ventura, CA (2011).
[14] Engine Combustion Network website: http://www.sandia.gov/ecn/index.php
[15] Kak, A. and Slaney, M., *Principles of Computerized Tomographic Imaging*, IEEE Press, New York (1998).
[16] Pope, S., *Turbulent Flows*, Cambridge University Press, New York (2000).
[17] Siebers, D., *SAE Paper 1999-01-0528* (1999).